# THE EFFECT OF MESA DIMENSIONS ON MEMS DIAPHRAGMS FOR FABRY-PEROT INTERFEROMETER-BASED FIBER OPTIC SENSORS

*Ahmet DURMAZ* [*] (ID)
*Şekip Esat HAYBER* [**] (ID)
*Umut AYDEMİR* [***] (ID)

**Abstract:** In this study, the effects of mesa dimensions on sensor response in diaphragm-based Fabry-Perot fiber optic sensors (FOSs) were investigated in detail. Mesa diaphragms, also called center-embossed diaphragms, have been discussed sufficiently in the literature, but the effect of mesa thickness on sensor performance has not been discussed in detail. Moreover, there is no precise analytical solution for such diaphragms. For this reason, diaphragms with different thicknesses and radii were selected, and the deflection and frequency responses of the diaphragm according to the applied acoustic pressure were analyzed using the ANSYS software, depending on whether the mesa is thinner or thicker than the diaphragm. If the thickness of the mesa is smaller than the thickness of the diaphragm, the center deflection changes drastically. However, if the thickness of the mesa is two times greater than the thickness of the diaphragm, there is no significant change in the deflection results. Similarly, if the mesa thickness is thinner than the diaphragm, the sensor's frequency response changes drastically with increasing mesa radius. In cases where the mesa thickness is larger than the diaphragm thickness, the frequency response changes less. According to the results, mesa dimensions should be considered when designing a mesa diaphragm-based Fabry-Perot FOS.

**Keywords:** Mesa Diaphragm, MEMS, Fabry-Perot Interferometer, Fiber Optic Sensors.

### Fabry-Perot İnterferometre Tabanlı Sensörlerde Mesa Boyutlarının MEMS Diyaframlar Üzerine Etkisi

**Öz:** Bu çalışmada diyafram tabanlı Fabry-Perot boşluklu fiber optik sensörlerde mesa boyutlarının sensör tepkisine etkileri detaylı olarak incelenmiştir. Literatürde ortası yükseltilmiş veya mesa olarak adlandırılan diyaframlar yeterince tartışılmış fakat mesa kalınlığının sensör performansına etkisi detaylı tartışılmamıştır. Bu tarz diyaframların kesin analitik çözümü ise bulunmamaktadır. Bu nedenle farklı kalınlık ve yarıçapa sahip diyaframlar seçilerek mesanın diyaframdan ince olması ve kalın olması durumlarına göre diyaframın, uygulanan akustik basınca göre esneme ve frekans tepkileri ANSYS programı kullanılarak analiz edilmiştir. Mesanın kalınlığı diyaframın kalınlığından küçük olması durumunda merkez esnemesi ciddi olarak değişmektedir. Ancak mesa kalınlığının diyaframın kalınlığından 2 kat büyük olması durumunda ise esneme sonuçlarında ciddi bir değişim olmamaktadır. Benzer şekilde mesa kalınlığının diyaframdan ince olması durumda sensörün frekans cevabı artan mesa yarıçapı ile ciddi olarak değişmektedir. Mesa kalınlığının diyafram kalınlığından daha büyük olduğu durumlarda ise frekans cevabı daha az değişmektedir. Elde edilen sonuçlara göre mesa diyafram tabanlı Fabry-Perot boşluklu fiber optik sensör tasarlanırken mesa boyutları dikkate alınmalıdır.

**Anahtar Kelimeler:** Mesa Diyafram, MEMS, Fabry-Perot İnterferometresi, Fiber Optik Sensör.

---

*   Optics and Photonics Engineering, Bursa Uludag University, 16120, Bursa, Türkiye.
**  Electrical-Electronics Engineering, Bursa Uludag University, 16120, Bursa, Türkiye.
***Electrical-Electronics Engineering, Bursa Uludag University, 16120, Bursa, Türkiye.
    Corresponding Author: Umut Aydemir (umutaydemir@uludag.edu.tr)

## 1. INRODUCTION

Fiber optic sensors (FOSs) have a wide dynamic range, high sensitivity, electrical isolation, small size, and resist harsh environments (Nuclear Regulatory Commission, 1994, Lű, 2015). Thanks to these advantages, it has broad application areas. Some of these application areas are temperature sensing in composite materials (Ramakrishnan et al., 2016), triaxial strain measurement (Mawatari et al., 2008), underwater acoustic applications (Cranch et al., 2003), biomedical applications (Tosi et al., 2018), aero-engine application (Fernández et al., 2021), smart textile applications (El-Sherif et al., 2000), structural health monitoring (Alwis et al., 2021), space applications (Jin et al., 2020), marine environment and marine structural health monitoring (Min et al., 2021), biogas reactors (Şahin & Khyber 2021), power transformer monitoring (Betta et al., 2001). Since the detection is done through light in FOSs, the measurement speed and continuous sampling make them the main reason for preference. FOSs are designed in different configurations according to the parameter to be measured (Sripriya & Jeyalakshmi, 2007). The most sensitive sensing configuration is the interferometric one among the FOSs. FOSs with Fabry-Perot interferometers (FPIs) are the most sensitive among them.

Pressure sensors based on the FPI have shown promising results for obtaining static and dynamic pressure measurements. Many studies were carried out with diaphragms with different geometric dimensions and made of different materials (Sun et al., 2007, Chin et al., 2007, Totsu et al., 2004). The sensors spread over an extensive area such as biomedical (Poeggel et al., 2015), gas detection (Gong et al., 2018), underwater applications (Wang et al., 2014), infrasound (Liao et al., 2017), and ultrasound applications (Rong et al., 2017), acoustics (Mao et al., 2017), pressure (Xu et al., 2012), acoustic pressure (Cheng et al., 2015), partial discharge in power transformers (Deng et al., 2001). These sensors consist of a fiber end surface and a diaphragm sensitive to the acoustic signal (Hayber et al., 2018). Acoustic pressure sensors are being investigated extensively (Wang et al., 2014). Among the factors determining the pressure sensitivity of Fabry-Perot sensors are the diaphragm material and the dimensions. The light from the optical fiber is modulated and detected by the deflection of the diaphragm under pressure.

Misalignment between the fiber and the diaphragm during manufacture causes uncertainty in the light intensity reflected into the fiber. An embossment added to the diaphragm increases the flatness in the middle of the diaphragm. In this case, the loss of light reflected from the diaphragm is reduced (Sun et al., 2008). Although analytical solutions have been described for flat diaphragm sensors, there is no complete analytical solution including all mesa parameters for mesa diaphragms. In the study of Padron et al., an analytical model is valid when the mesa thickness is at least six times greater than the diaphragm thickness. In the study of Sun et al., a design guideline is given for cases where the thickness of the mesa is not greater than the thickness of the diaphragm. The study made by Ge et al. differs from models discussed by Padron et al. and Sun et al. with an unconditional analytical model that includes all diaphragm and mesa parameters. Since these analytical models are not precise and are obtained from certain approaches, they need simulation and experimental validation.

Moreover, a center-embossed MEMS structure was used in different studies such as pressure sensors (Ge et al., 2008, Yıldız, 2021), micro pressure sensors with a silicon diaphragm (Tian et al., 2018), catheter applications (Katsumata et al., 2000), FPIs (Padron et al., 2010), medical applications (Totsu et al., 2004). When all the literature is examined, there is no detailed frequency analysis of the mesa diaphragm's thickness according to the main diaphragm's thickness. In literature, a limited case was investigated by Sun et al. where the ratio of the mesa and the diaphragm's radius is 0.186. In addition, when the applied articles are examined, the mesa radius varies, but there is no detailed study to reveal the nature of the frequency response to these changes.

In the present study, the effects of mesa thickness and radius on MEMS diaphragms were investigated by ANSYS simulations. Static structural and modal analyses are conducted to

understand mesa diaphragms' deflection and frequency response. There are different numerical approaches related to the deformation of mesa-structured diaphragms. The existence of different models in the literature to analyze the deflection of center-embossed diaphragms reveals the necessity of verifying these results with simulation or experimental results. The effect of mesa thickness and radius on deflection has been analyzed from thin to thick mesa dimensions. The frequency response of the different mesa dimensions is also obtained for MEMS diaphragms as a novel. The presented study analyzes in detail that the frequency response may differ. In our study, the cases where the mesa and diaphragm thickness ratio is less than one and greater than one are shared with the literature.

## 2. MATERIAL AND METHOD

### 2.1. FPI with Mesa Diaphragm

The system shown in Figure 1 consists of a sensor tip, a semiconductor light emitter that can operate at different wavelengths, an optical receiver, and fibers that connect components. The 2×1 fiber coupler is used to transmit light to the diaphragm and transmit reflected light to the detector. The incidence light is first reflected from the end of the fiber. The remaining light passes through the air gap and is partially reflected from the diaphragm surface. As seen in Figure1a and Figure 1b, these multiple reflections reach the optical receiver over the same fiber.
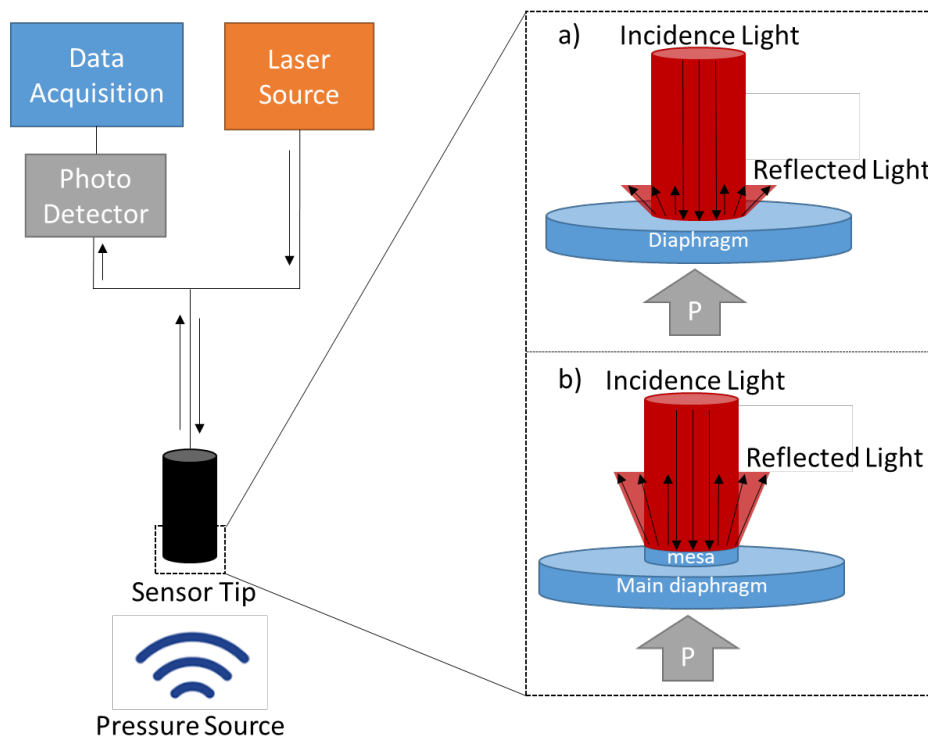


***Figure 1:***
*Schematic representation of MEMS diaphragm-based fiber optic Fabry-Perot Interferometric sensor structure;*
***a.** Conventional diaphragm, **b.** Mesa diaphragm*

Center deflection and frequency response are two essential characteristics of a diaphragm (S. E. Hayber et al., 2019). The diaphragm vibrates in a specific resonance frequency range in response to the applied pressure. This vibration is detected in the photodetector by reflecting a laser beam sent from the other side of the diaphragm. The illustration of the sensing mechanism

is given in Figure 1a and Figure1b. The mesa structure provides the advantage of flatness in the center of the diaphragm (Ge et al., 2008) (Ge et al., 2016). However, not considering the dimensions of the mesa structure in the design can be a disadvantage to the sensor's sensitivity (Ş. E. Hayber & Aydemir, 2021). For this reason, the effects of mesa dimensions on the sensor response were examined in detail in this study.

For ANSYS simulations, silica (E=73GPa, μ=0.17, d=2200kg/m$^3$) is selected both for the mesa and main diaphragm. Mesh settings are selected as resolution '2' by activating the program-controlled "adaptive sizing" option. At the same time, the transition option has been set to 'slow' to get more precise results. Dimensions of diaphragm parameters used in this study are given in Table 1. In Figure 2, $r_d$ and $r_m$ represent the diaphragm and mesa radius, and $t_d$ and $t_m$ represent the diaphragm and mesa thickness.
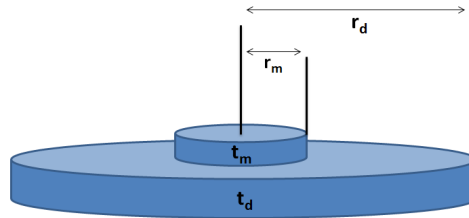


***Figure 2:***
*Mesa-Diaphragm structure and its parameters*

**Table 1. Dimensions of diaphragm parameters used in this study**

| Main Diaphragm Name | Main Diaphragm Dimension ($r_d, t_d$) | Variable Mesa Radius $r_m$ | Variable Mesa Thickness $t_m \leq t_d$ | Variable Mesa Thickness $t_m \geq t_d$ |
|---|---|---|---|---|
| MD1 | 100μm, 1μm | 0–90μm (10μm step) | 0.2μm–1μm (0.1μm step) | 1μm–10μm (1μm step) |
| MD2 | 300μm, 5μm | 0–270μm (30μm step) | 0.5μm–5μm (0.5μm step) | 5μm–50μm (5 interval) |
| MD3 | 500μm, 10μm | 0–450μm (50μm step) | 1μm–10μm (1μm step) | 10μm–100μm (10μm step) |

According to the analytical solution proposed by Padron et al., the thickness of the mesa should be at least six times greater than the thickness of the diaphragm (Padron et al., 2008). The deflection equation for a diaphragm under pressure is expressed in Equation 1. In the analytical solution proposed by Sun et al., the mesa thickness provides a solution for cases where the diaphragm thickness is less than six times (Sun et al., 2008). According to them, the deflection equation for a mesa diaphragm under pressure is expressed in Equation 2. In another model proposed by Ge et al., there is no prerequisite, and the analytical solution includes the mesa thickness, unlike the other solutions above, as seen in Equation 3 (Ge et al., 2008). In this context, the simulation results are compared with this Equation 3.

$$W_1 = A_P \frac{P}{E} \frac{(2r_d)^4}{t_d^3} \tag{1}$$

$$W_2 = A_P \frac{P\, r_d{}^4}{E\, t_d{}^3}$$

$$A_p = \frac{3(1 - \mu^2)}{16}\left(1 - \frac{r_m^4}{r_d^4} - 4\frac{r_m^2}{r_d^2}\log\frac{r_d}{r_m}\right)$$

(2)

$$W_3 = P\left(\frac{r_d^4 - r_m^4}{64D_2} + \frac{r_m^4}{64D_1} + \frac{r_d^2 r_m^2}{16D_2}\frac{r_m}{r_d}\right)$$

$$D_1 = \frac{E(t_d + t_m)^3}{12(1 - \mu^2)} \quad D_2 = \frac{Et_d^3}{12(1 - \mu^2)}$$

(3)

Here E is the Young modulus, μ is the Poisson's ratio, and P is applied pressure. Diaphragm parameters used in the equations can be seen in Figure 2.

Frequency response is vital in determining the frequency range in which the acoustic wave will be detected. While there is an analytical solution in the literature for conventional diaphragms (Hayber et al., 2018), there is no analytical approach for calculating the resonance frequency for mesa diaphragms.

## 3. RESULTS AND DISCUSSION

Since conventional diaphragms are deflected by a radius of curvature depending on applied pressure, the researchers used mesa diaphragms to flatten the center of the diaphragm. These processes are optimized carefully to detect acoustic signals with minimum loss. The results of ANSYS static structural and modal simulation are given in Figure 3a and Figure 3b, respectively. Figures correspond to one of the simulated mesa diaphragms ($r_d$=300μm, $r_m$=150μm, $t_d$=5μm, $t_m$=10μm) made by $SiO_2$ under 1Pa pressure. The simulations are repeated by changing the parameters of the main diaphragm and mesa for the same material and pressure. Since deflection results represent sensor sensitivity in the FPI, these results are examined in detail.

Firstly, Figure 4 was obtained to understand the effect of the mesa radius as thinner than the diaphragm and thicker than the diaphragm for three different main diaphragm sizes (MD1, MD2, MD3) with Ansys Static Structural analysis. The figure shows the change in the varying mesa dimensions while remaining constant in diaphragm dimensions. Figure 4 shows the mesa diaphragm's sensitivity (nm/kPa) depending on the change in the radius of the mesa. Since the sensitivity is S=d/P, it is directly proportional to the deflection in the center. In the analysis, the cases of mesa thickness being smaller and larger than the main diaphragm thickness were examined separately.

Accordingly, Figure 4.a-c shows the first case where the mesa thickness is smaller than the main diaphragm. The main diaphragm thickness was chosen as 1μm, 5μm, and 10μm values for MD1, MD2, and MD3, respectively. Thus, the behavior of both very thin diaphragm structures and average thickness values will be understood. In all thickness values, it is observed that the sensitivity decreases with increasing the mesa radius as a general nature. In addition, the effect of mesa radius on sensitivity increases with increasing mesa thickness. Increasing the radius in thick mesa structures decreases the sensitivity rapidly. When the mesa thickness is 0.5μm, the dynamic range of sensitivity changes from 160nm/kPa to 140nm/kPa, with a change of 20nm/kPa for the D2 diaphragm seen in Figure 4b. Whereas when the mesa thickness is 4.5μm for the same diaphragm, the dynamic range of sensitivity changes from 160nm/kPa to 40nm/kPa with a change of 120nm/kPa. In addition, as can be seen from the analysis results, this change differs in different mesa thicknesses. Similar results apply to the MD1 and MD3 given in Figure 4a and Figure 4c, respectively.
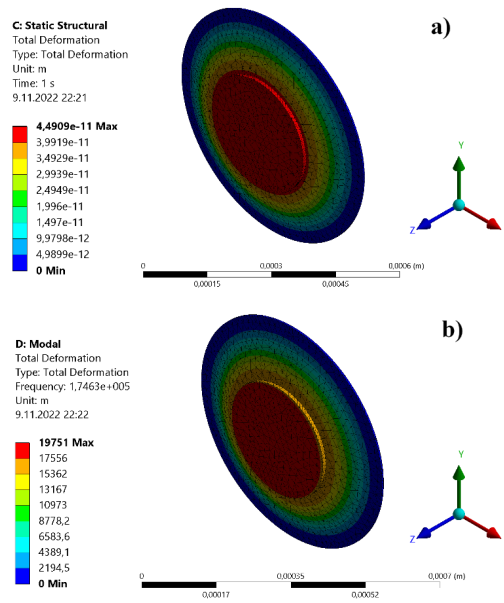
***Figure 3:***
*Isometric view of the simulated mesa diaphragm ($r_d$=300μm, $r_m$=150μm, $t_d$=5μm, $t_m$=10μm);*
***a.*** *Static Structural,* ***b.*** *Modal Analysis*

To better explain the effect of mesa thickness on the deflection behavior, $r_m = r_d/2$ is selected, and simulation and analytical solutions are compared for MD1, MD2, and MD3 diaphragms in Table 2, Table 3, and Table 4, respectively. As seen from the tables and comparison graphs, in the case of $t_m < t_d$, the diaphragm's response changes drastically even at very thin mesa thicknesses. However, the current analytical model, which gives more accurate results for thick mesa structures, does not allow researchers to see this change.

Figure 4d-f shows the second case where the thickness of the mesa is greater than the thickness of the main diaphragm. Similar to the first case, increasing the radius of the mesa tends to decrease the sensitivity. It has been observed that the dynamic range in all cases where the thickness of the mesa is twice the thickness of the main diaphragm remains almost the same in all cases. This result supports the conclusion suggested by Padron et al. that the mesa effect can be neglected if the mesa thickness is greater than the diaphragm thickness. According to this approach, the mesa thickness may be negligible in some cases, but the diaphragm deflection falls drastically with increasing mesa radius. It can be concluded that the mesa thickness should be kept lower than the diaphragm thickness in cases where sensitivity needs to be adjusted. As can be seen from the Table 2, Table 3, and Table 4 for MD1, MD2, and MD3 and its comparison graphs obtained for $r_m = r_d/2$, the mesa effect can be neglected when $t_m > 2t_d$.
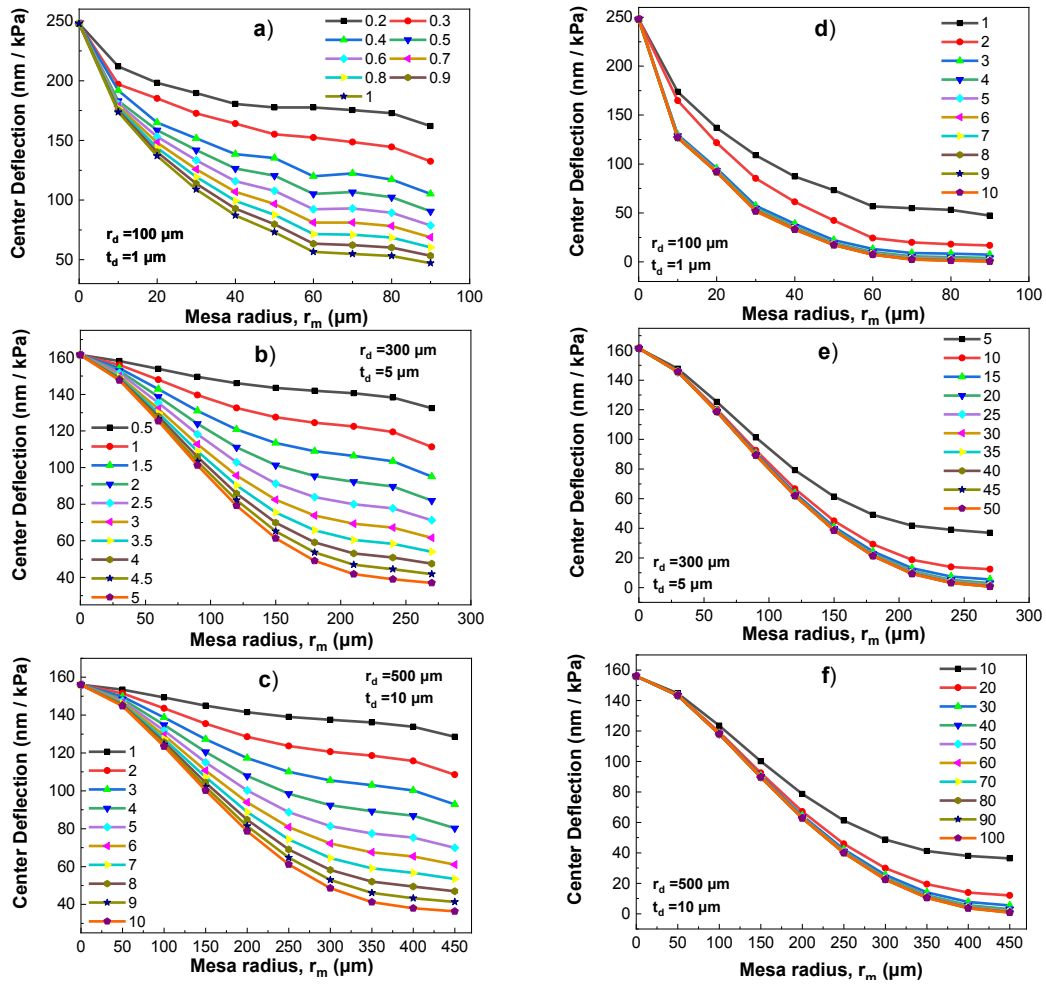
***Figure 4:***
*Center deflection vs. mesa radius plots with varying $t_m$ **a.-c.** for $t_m < t_d$, and **d.-f.** for $t_m > t_d$*

**Table 2. The comparison of analytical and simulation results for MD1**

| $t_m$ (µm) | Simulation Results | Analytical Results | Graphical Comparison ($r_d$=100µm, $r_m$=50µm, $t_d$=1µm) |
|---|---|---|---|
| 0.1 | 1.758E-10 | 1.705E-10 | |
| 0.2 | 1.777E-10 | 1.678E-10 | |
| 0.3 | 1.552E-10 | 1.659E-10 | |
| 0.4 | 1.352E-10 | 1.644E-10 | |
| 0.5 | 1.205E-10 | 1.634E-10 | |
| 0.6 | 1.077E-10 | 1.626E-10 | |
| 0.7 | 9.682E-11 | 1.619E-10 | |
| 0.8 | 8.761E-11 | 1.614E-10 | |
| 0.9 | 7.975E-11 | 1.610E-10 | |
| 1 | 7.314E-11 | 1.607E-10 | |
| 2 | 4.233E-11 | 1.593E-10 | |
| 3 | 2.224E-11 | 1.590E-10 | |
| 4 | 1.931E-11 | 1.589E-10 | |
| 5 | 1.827E-11 | 1.588E-10 | |
| 6 | 1.783E-11 | 1.588E-10 | |
| 7 | 1.757E-11 | 1.588E-10 | |
| 8 | 1.737E-11 | 1.588E-10 | |
| 9 | 1.724E-11 | 1.588E-10 | |
| 10 | 1.713E-11 | 1.588E-10 | |

**Table 3. The comparison of analytical and simulation results for MD2**

| $t_m$ (µm) | Simulation Results | Analytical Results | Graphical Comparison ($r_d$=300µm, $r_m$=150µm, $t_d$=5µm) |
|---|---|---|---|
| 0.5 | 1.436E-10 | 1.105E-10 | |
| 1 | 1.276E-10 | 1.087E-10 | |
| 1.5 | 1.134E-10 | 1.075E-10 | |
| 2 | 1.014E-10 | 1.066E-10 | |
| 2.5 | 9.129E-11 | 1.059E-10 | |
| 3 | 8.243E-11 | 1.053E-10 | |
| 3.5 | 7.553E-11 | 1.049E-10 | |
| 4 | 6.988E-11 | 1.046E-10 | |
| 4.5 | 6.523E-11 | 1.043E-10 | |
| 5 | 6.141E-11 | 1.041E-10 | |
| 10 | 4.491E-11 | 1.033E-10 | |
| 15 | 4.100E-11 | 1.030E-10 | |
| 20 | 3.971E-11 | 1.030E-10 | |
| 25 | 3.909E-11 | 1.029E-10 | |
| 30 | 3.883E-11 | 1.029E-10 | |
| 35 | 3.867E-11 | 1.029E-10 | |
| 40 | 3.870E-11 | 1.029E-10 | |
| 45 | 3.859E-11 | 1.029E-10 | |
| 50 | 3.852E-11 | 1.029E-10 | |

**Table 4. The comparison of analytical and simulation results for MD3**

| $t_m$ ($\mu$m) | Simulation Results | Analytical Results | Graphical Comparison ($r_d$=500$\mu$m, $r_m$=250$\mu$m, $t_d$=10$\mu$m) |
|---|---|---|---|
| 1 | 1.391E-10 | 1.065E-10 | |
| 2 | 1.237E-10 | 1.049E-10 | |
| 3 | 1.100E-10 | 1.037E-10 | |
| 4 | 9.842E-11 | 1.028E-10 | |
| 5 | 8.878E-11 | 1.021E-10 | |
| 6 | 8.084E-11 | 1.016E-10 | |
| 7 | 7.435E-11 | 1.012E-10 | |
| 8 | 6.905E-11 | 1.009E-10 | |
| 9 | 6.471E-11 | 1.006E-10 | |
| 10 | 6.115E-11 | 1.004E-10 | |
| 20 | 4.592E-11 | 9.958E-11 | |
| 30 | 4.229E-11 | 9.937E-11 | |
| 40 | 4.107E-11 | 9.930E-11 | |
| 50 | 4.052E-11 | 9.927E-11 | |
| 60 | 4.028E-11 | 9.925E-11 | |
| 70 | 4.011E-11 | 9.924E-11 | |
| 80 | 4.002E-11 | 9.923E-11 | |
| 90 | 3.998E-11 | 9.923E-11 | |
| 100 | 3.994E-11 | 9.923E-11 | |
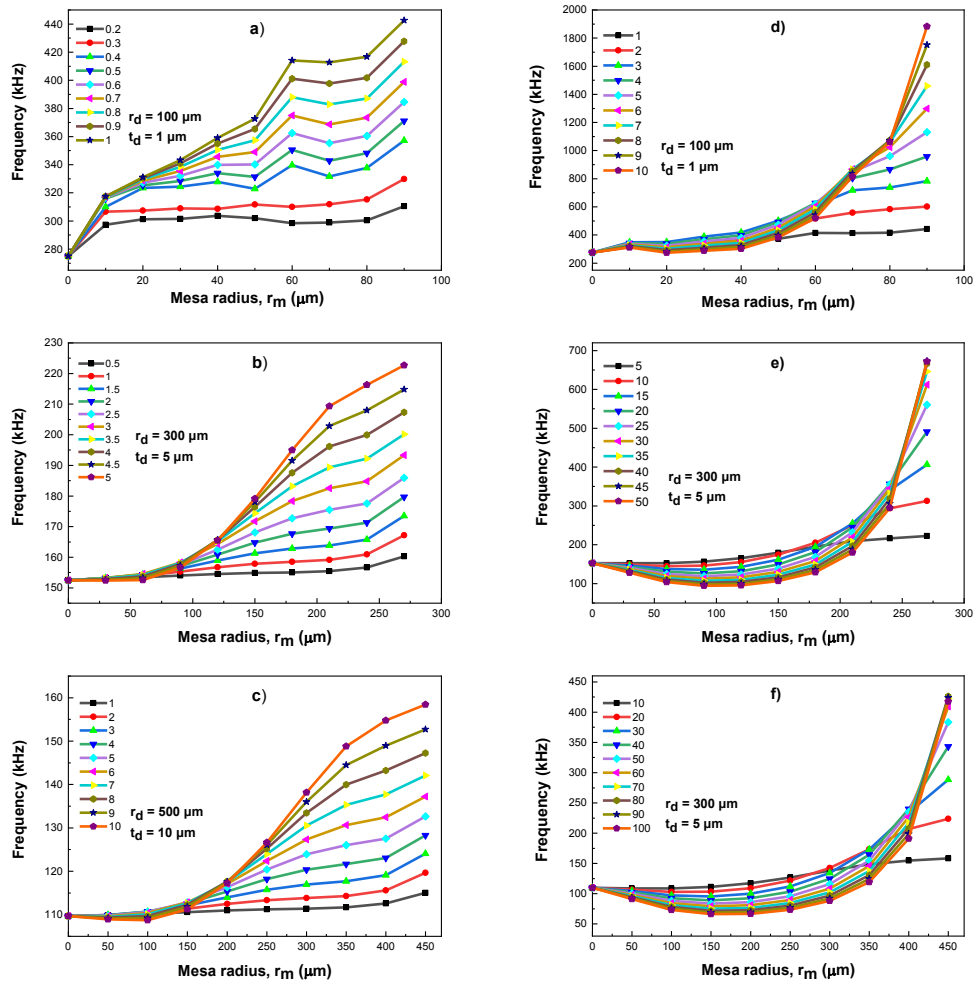
***Figure 5:***
*Frequency vs. mesa radius plots with varying;*
***a.-c.*** *for $t_m < t_d$, and* ***d.-f.*** *for $t_m > t_d$*

Contrary to deflection, there is not even an approximate analytic solution for the frequency response of mesa diaphragms in the literature. Figure 5 shows the frequency response of the mesa diaphragm depending on the change in the mesa radius. In the analysis, the cases of mesa thickness being smaller and larger than the main diaphragm thickness were examined separately. Mesa-induced varying frequency response analysis was investigated for three main diaphragms.

Figure 5a-c shows the first case where the mesa thickness is smaller than the main diaphragm. In all thickness values, the diaphragm's frequency response did not significantly change and remained constant until a certain radius value, depending on the increase in the radius of the mesa as a general nature. After this certain radius value, it showed an increasing trend. In addition, the effect of mesa radius on frequency response increases with increasing mesa thickness. Increasing the radius in thick mesa structures increases the frequency rapidly. When the mesa thickness is 0.5µm, the dynamic range of frequency response changes from 152kHz to 160kHz, with a change of 8kHz for the MD2 diaphragm seen in Figure 5b. Whereas when the mesa thickness is 4.5µm for the same diaphragm, the dynamic range of sensitivity changes from 152kHz to 215kHz with a change of 63kHz. Similar discussions can be made in Figure 5a and Figure 5c, but there are some differences in the frequency response, which remains constant up to a certain radius value. In Figure 5a, the frequency response immediately

187

starts to change depending on the increasing radius of the mesa. At the same time, the behavior is different in Figure 5b and Figure 5c. In Figure 5b, a change in frequency is observed when the mesa radius is larger than approximately 75μm, whereas in Figure 5c, a change in frequency response is observed when the mesa radius is larger than approximately 150μm. After these certain radius values, these changes differ significantly at different mesa thickness values.

Figure 5d-f shows the second case where the thickness of the mesa is greater than the thickness of the main diaphragm. In this case, a predictable behavior cannot be exhibited depending on the change in mesa thickness. The frequency response at different mesa thicknesses decreases to a certain radius value depending on the increasing radius and then tends to increase. In addition, the responses are like each other at varying thickness values. This situation is similar to the result of the sensitivity analysis. Accordingly, this second case is not valid where frequency response adjustments are needed.

## 4. CONCLUSIONS

This study analyzes the deflection and frequency response of the mesa diaphragms in detail depending on the different mesa thickness, mesa radius, diaphragm thickness, and diaphragm radius. While mesa diaphragms do not have an exact analytical solution in the literature, they are used to reduce sensor losses. Mesa diaphragm structures are often produced on demand, but sometimes they are formed when trying to coat very thin reflective metal. In the case of $t_m < t_d$, mesa-induced deflection changes are neglected in the literature for FPIs. For this reason, according to ANSYS simulation results, there is a severe decrease in the center deflection of the sensor in the case of $t_m < t_d$ at different mesa thicknesses. This decrease in deflection directly indicates the loss of sensitivity of the sensor. Similarly, in the case of $t_m < t_d$, the sensor's frequency response also increases significantly with increasing mesa thickness and radius. In addition, the $t_m > t_d$ case has been examined separately with simulations, and the sensor's sensitivity does not cause a severe change when $t_m > 2t_d$. However, while the mesa thickness is neglected in the literature, the radius of the mesa affects the sensitivity quite a lot, and it should be considered. It was concluded that changing mesa sizes caused less changes in frequency response.

In this study, it is concluded that the sensitivity and frequency response of the diaphragm can be adjusted in the FPI according to the mesa dimensions. In addition, the results obtained can guide applications other than the FPI, where a mesa diaphragm is needed.

## CONFLICT OF INTEREST

The authors declare no conflict of interest.

## AUTHOR CONTRIBUTION

Ahmet Durmaz carried out the simulations and visualization; Şekip Esat Hayber and Umut Aydemir conceptualized the study and wrote the article.

## KAYNAKLAR

1.  Alwis, L. S., Bremer, K., & Roth, B. (2021). Fiber optic sensors embedded in textile-reinforced concrete for smart structural health monitoring: A review. *Sensors*, 21(15), 4948. doi:10.3390/s21154948.

2.  Betta, G., Pietrosanto, A., & Scaglione, A. (2001). An enhanced fiber-optic temperature sensor system for power transformer monitoring. *IEEE Transactions on instrumentation and measurement*, 50(5), 1138-1143. doi:10.1109/19.963173.

3.  Cheng, L., Qianwen, L., Tingting, G., Jun, X., Shangchun, F., & Wei, J. (2015, November). An ultra-high sensitivity Fabry-Perot acoustic pressure sensor using a multilayer suspended graphene diaphragm. In 2015 *IEEE SENSORS* (pp. 1-4). IEEE. doi:10.1109/ICSENS.2015.7370318.

4.  Chin, K. K., Sun, Y., Feng, G., Georgiou, G. E., Guo, K., Niver, E., ... & Noe, K. (2007). Fabry-Perot diaphragm fiber-optic sensor. *Applied optics*, 46(31), 7614-7619. doi:10.1364/AO.46.007614.

5.  Cranch, G. A., Nash, P. J., & Kirkendall, C. K. (2003). Large-scale remotely interrogated arrays of fiber-optic interferometric sensors for underwater acoustic applications. *IEEE Sensors Journal*, 3(1), 19-30. doi:10.1109/JSEN.2003.810102.

6.  Deng, J., Xiao, H., Huo, W., Luo, M., May, R., Wang, A., & Liu, Y. (2001). Optical fiber sensor-based detection of partial discharges in power transformers. *Optics & Laser Technology*, 33(5), 305-311. doi:10.1016/S0030-3992(01)00022-6.

7.  El-Sherif, M. A., Yuan, J., & MacDiarmid, A. (2000). Fiber optic sensors and smart fabrics. *Journal of intelligent material systems and structures*, 11(5), 407-414. doi:10.1106/MKNK-E482-GWUG-0HE7.

8.  Fernández, R., Amorebieta, J., García, I., Aldabaldetreku, G., Zubia, J., & Durana, G. (2021). Review of a custom-designed optical sensing system for aero-engine applications. International *Journal of Turbomachinery, Propulsion and Power*, 6(1), 3. doi:10.3390/ijtpp6010003.

9.  Ge, Y. X., Wang, M., & Yan, H. T. (2008, November). Mesa diaphragm-based Fabry-Perot optical MEMS pressure sensor. In *2008 1st Asia-Pacific Optical Fiber Sensors Conference* (pp. 1-4). IEEE. doi:10.1109/APOS.2008.5226325.

10. Ge, Y., Wang, M., Rong, H., & Chen, X. (2008, January). A novel optical MEMS pressure sensor with a mesa diaphragm. In *MEMS/MOEMS Technologies and Applications III* (Vol. 6836, pp. 232-240). SPIE. doi:10.1117/12.755190.

11. Ge, Y., Wang, T., Zhang, J., & Chang, J. (2016). Wavelength-demodulation MEMS Fabry Perot temperature sensor based on bimetallic diaphragm. *Optik*, *127*(12), 5040-5043. doi:10.1016/j.ijleo.2016.02.050.

12. Gong, Z., Chen, K., Yang, Y., Zhou, X., & Yu, Q. (2018). Photoacoustic spectroscopy based multi-gas detection using high-sensitivity fiber-optic low-frequency acoustic sensor. *Sensors and Actuators B: Chemical*, 260, 357-363. doi:10.1016/j.snb.2018.01.005.

13. Hayber, S. E., Tabaru, T. E., & Saracoglu, O. G. (2019). A novel approach based on simulation of tunable MEMS diaphragm for extrinsic Fabry–Perot sensors. *Optics Communications*, *430*, 14-23. doi:10.1016/j.optcom.2018.08.021.

14. Hayber, Ş. E., & Aydemir, U. (2021). Design and simulation of a novel fungus-shaped center embossed diaphragm for fiber optic pressure sensors. *Optical Fiber Technology*, *61*, 102429. doi:10.1016/j.yofte.2020.102429.

15. Hayber, Ş. E., Tabaru, T. E., Aydemir, U., & Saraçoğlu, Ö. G. (2018). Fiber Optik Fabry-Perot Akustik Sensörler için Yeni Bir Diyafram Malzemesi Olarak 2D GaSe Benzetimi. *Düzce Üniversitesi Bilim ve Teknoloji Dergisi*, *6*(2), 369-381..

16. Jin, J., He, J., Song, N., Ma, K., & Kong, L. (2020). A compact four-axis interferometric fiber optic gyroscope based on multiplexing for space application. *Journal of Lightwave Technology*, 38(23), 6655-6663. doi:10.1109/JLT.2020.3015713.

17. Katsumata, T., Haga, Y., Minami, K., & Esashi, M. (2000). Micromachined 125μm diameter ultra miniature fiber-optic pressure sensor for catheter. *IEEJ Transactions on Sensors and Micromachines*, 120(2), 58-63. doi:10.1541/ieejsmas.120.58.

18. Liao, H., Lu, P., Liu, L., Wang, S., Ni, W., Fu, X., ... & Zhang, J. (2017). Phase demodulation of short-cavity Fabry–Perot interferometric acoustic sensors with two wavelengths. *IEEE Photonics Journal*, 9(2), 1-9. doi:10.1109/JPHOT.2017.2689771.

19. Lű, T. (2015). Influence of cavity loss on an extrinsic Fabry-Perot cavity intensity-based pressure sensor. *Review of Scientific Instruments*, *86*(9), 095002. doi:10.1063/1.4929681.

20. Mao, X., Yuan, S., Zheng, P., & Wang, X. (2017). Stabilized fiber-optic Fabry–Perot acoustic sensor based on improved wavelength tuning technique. *Journal of Lightwave Technology*, 35(11), 2311-2314.

21. Mao, X., Yuan, S., Zheng, P., & Wang, X. (2017). Stabilized fiber-optic Fabry–Perot acoustic sensor based on improved wavelength tuning technique. *Journal of Lightwave Technology*, 35(11), 2311-2314.

22. Min, R., Liu, Z., Pereira, L., Yang, C., Sui, Q., & Marques, C. (2021). Optical fiber sensing for marine environment and marine structural health monitoring: A review. *Optics & Laser Technology*, 140, 107082. doi:10.1016/j.optlastec.2021.107082.

23. Nuclear Regulatory Commission. (1994). *Transactions of the twenty-second water reactor safety information meeting* (No. NUREG/CP--0139). Nuclear Regulatory Commission.

24. Padron, I., Fiory, A. T., & Ravindra, N. M. (2008). Modeling and design of an embossed diaphragm fabry-perot pressure Sensor. In *Mater. Sci. Technol. Conf. Exhib. MS T* (Vol. 8, pp. 992-997).

25. Padron, I., Fiory, A. T., & Ravindra, N. M. (2010). Novel MEMS Fabry-Perot interferometric pressure sensors. In *Materials Science Forum* (Vol. 638, pp. 1009-1014). Trans Tech Publications Ltd. doi:10.4028/www.scientific.net/MSF.638-642.1009.

26. Poeggel, S., Tosi, D., Duraibabu, D., Leen, G., McGrath, D., & Lewis, E. (2015). Optical fibre pressure sensors in medical applications. *Sensors*, 15(7), 17115-17148. doi:10.3390/s150717115.

27. Ramakrishnan, M., Rajan, G., Semenova, Y., & Farrell, G. (2016). Overview of fiber optic sensor technologies for strain/temperature sensing applications in composite materials. *Sensors*, 16(1), 99. doi:10.3390/s16010099.

28. Rong, Q., Hao, Y., Zhou, R., Yin, X., Shao, Z., Liang, L., & Qiao, X. (2017). UW imaging of seismic-physical-models in air using fiber-optic Fabry-Perot interferometer. *Sensors*, 17(2), 397. doi:10.3390/s17020397.

29. Sripriya, T., & Jeyalakshmi, V. (2007). International Conference on Signal Processing, Embedded System and Communication Technologies and their applications for Sustainable and Renewable Energy (ICSECSRE' 14) Simulation of an Optical MEMS pressure sensor. In *International Journal of Advanced Research in Electrical, Electronics and Instrumentation Engineering An ISO* (Vol. 3297, Issue 3).

**30.** Sun, Y., Feng, G., Georgiou, G., Niver, E., Noe, K., & Chin, K. (2008). Center embossed diaphragm design guidelines and Fabry–Perot diaphragm fiber optic sensor. *Microelectronics journal*, *39*(5), 711-716. doi:10.1016/j.mejo.2007.12.020.

**31.** Sun, Y., Feng, G., Georgiou, G., Padron, I., Niver, E., Noe, K., & Chin, K. K. (2007). Fabry-Perot Diaphragm Fiber Optic Sensor (DFOS) for Acoustic Detection. *Sensor and Transducer Journal*, Special Issue, 76-83.

**32.** Şahin, M., & Hayber, Ş. E. (2021). Fiber optic sensor design and prototyping for humidity detection in biogas reactors. *Politeknik Dergisi*, 1-1. doi:10.2339/politeknik.904631.

**33.** Tian, B., Zhan, F., Han, F., Li, K., Zhao, N., Yang, N., & Jiang, Z. (2018). An optical fiber Fabry–Pérot micro-pressure sensor based on beam-membrane structure. *Measurement Science and Technology*, 29(12), 125104. doi:10.1088/1361-6501/aadfb1.

**34.** Tosi, D., Poeggel, S., Iordachita, I., & Schena, E. (2018). Fiber optic sensors for biomedical applications. In *Opto-mechanical fiber optic sensors* (pp. 301-333). Butterworth-Heinemann.

**35.** Totsu, K., Haga, Y., & Esashi, M. (2004). Ultra-miniature fiber-optic pressure sensor using white light interferometry. *Journal of Micromechanics and Microengineering*, 15(1), 71. doi:10.1088/0960-1317/15/1/011.

**36.** Totsu, K., Haga, Y., & Esashi, M. (2004). Ultra-miniature fiber-optic pressure sensor using white light interferometry. *Journal of Micromechanics and Microengineering*, 15(1), 71. doi:10.1088/0960-1317/15/1/011.

**37.** Xu, F., Ren, D., Shi, X., Li, C., Lu, W., Lu, L., ... & Yu, B. (2012). High-sensitivity Fabry–Perot interferometric pressure sensor based on a nanothick silver diaphragm. *Optics letters*, 37(2), 133-135. doi:10.1364/OL.37.000133.

**38.** Yildiz, F. (2021). Comparison of Two Different Circular Diaphragm Models with Central Mass for MEMS Based FPI Pressure Sensor Performance Based on Sensitivity and Frequency Response. *Sakarya University Journal of Science*, *25*(3), 619-628.